Electrospinning-derived “Hairy Seaweed” and its photoelectrochemical properties

Kong, Junhua; Wei, Yuefan; Yang, Liping; Yee, Wu Aik; Dong, Yuliang; Zhou, Rui; Wong, Siew Yee; Ke, Lin; Sun, Xiaowei; Du, Hejun; Li, Xu; Lu, Xuehong

2013

Kong, J., Wei, Y., Yang, L., Yee, W., Dong, Y., Zhong, R., et al. (2013). Electrospinning-Derived “Hairy Seaweed” and Its Photoelectrochemical Properties. Journal of Physical Chemistry C, 117(19), 10106–10113.

https://hdl.handle.net/10356/96654

https://doi.org/10.1021/jp3125395

Electrospinning-Derived "Hairy Seaweed" and Its Photoelectrochemical Properties

*Junhua Kong,[a, §] Yuefan Wei,[b, §] Liping Yang,[a] Wu Aik Yee,[a] Yuliang Dong,[a] Rui Zhou,[a] Siew Yee Wong,[c] Lin Ke,[c] Xiao Wei Sun,[d] Hejun Du,[b] Xu Li,[c] Xuehong Lu[a, *]*

[a] School of Materials Science and Engineering, Nanyang Technological University, 50 Nanyang Avenue, Singapore 639798

[b] School of Mechanical and Aerospace Engineering, Nanyang Technological University, 50 Nanyang Avenue, Singapore 639798

[c] Institute of Materials Research & Engineering, A-star, 3 Research Link, Singapore 117602

[d] School of Electric and Electronic Engineering, Nanyang Technological University, 50 Nanyang Avenue, 639798, Singapore

KEYWORDS: electrospinning, nanofibers, zinc oxide, nanorods, photoelectrochemical

ABSTRACT: Highly porous three-dimensional (3D) hierarchical nanostructures suspended in aqueous media were facilely prepared via electrospinning of polyacrylonitrile (PAN)/indium tin oxide (ITO) nanofibers and collection of the hybrid nanofibers by water, followed by hydrothermally growing ZnO nanorods from the nanofibers. The large inter-fiber distances facilitated the uniform growth of the ZnO nanorods throughout the whole system. The suspended PAN/ITO nanofibers process excellent light trapping capability due to their centimeter-sized dimensions and hence large light penetration path. This significantly increases the probability of multiple-reflections, leading to high absorption with almost zero transmission when the size of

the sample reaches 10 mm in the direction parallel to incident light. High photocurrent was generated when the nanorods-on-nanofibers was used as a photoanode. The high photocurrent density generated by the anode can be attributed to its excellent light-trapping capability brought by the large amount of interaction sites between the ZnO nanorods and light, its large contact area with electrolyte, as well as the conduction path constructed by high-content ITO nanoparticles.

Introduction

Utilization of sunlight as a clean energy source to generate electricity or hydrogen has recently emerged as a hot topic in both scientific and industrial fields owing to the urgent need for environment protection and rising energy demand. It is considered as one of the most promising techniques for clean energy generation.[1] In a typical photoelectrochemical (PEC) process, solar energy is absorbed by a photoelectrode and utilized to generate electricity or electrochemically split water into an important green energy source, hydrogen. Similar to other electrochemical devices, the morphology and material properties of the photoelectrode play essential roles in determining the performance of a PEC system.

In the past few years, great efforts have been made in tailoring photoelectrode morphologies of various PEC active materials, such as TiO_2, ZnO, WO_3, $BiVO_4$ and Fe_2O_3. Typical designs include mesoporous nanostructures,[2-5] porous mats composed of one-dimensional (1D) nanostructures (nanorods, nanowires and nanotubes),[6-13] thin films,[14-18] as well as nanopetals and nanocoral.[19, 20] The porous morphology could provide large contact area with electrolytes and therefore more reaction sites, while the nanometer-sized dimensions, especially 1D nanostructures, could significantly improve the efficiency of charge (holes and electrons)

separation and transport in the nanostructures. Another unique design that has attracted great attention recently is three-dimensional (3D) hierarchical morphologies, which have superior advantages over the others for the photoelectrodes. It is widely reported that nanorods/nanowires/nanotubes of ZnO, TiO_2 and Fe_2O_3 can be fabricated on various substrates, such as fluorine doped tin oxide glass substrate and silicon wafer, to form aligned arrays.[21-26] Recently, shorter nanorods of these transitional metal oxides have been successfully grown on 1D structures, for example, carbon and silicon fibers, and aligned arrays of metal oxide wires/rods, to form hierarchical nanostructures.[27-33] In such 3D hierarchical structures, the 1D skeletons facilitate charge carrier collection, while the large amount of branches provide fairly large surface area for effective light trapping and electrochemical reaction. However, an unsolved issue with these high-density 3D hierarchical nanostructures is that the path of light in the electrodes is typically at micrometer scale, which is constrained by the thickness of the compact nanofibrous mats or the length of the aligned metal oxide nanorod arrays in the direction of light incidence. This severely limits the interactions of active materials with light. Moreover, the growth of metal oxide nanorods on nanofibrous mats or parallel nanowire arrays is also largely constrained by the limited inter-spaces between the nanofibers/nanowires, for instance, the ones in the compact electrospun mats collected using a plate collector.[34] The growth mostly occurs on those nanofibers/nanowires that are located on the surface of the nanofibrous mats/nanowire arrays.

To address the above issues, in this work, loose agglomerate of polyacrylonitrile (PAN)/indium tin oxide (ITO) hybrid nanofibers, i.e. the so-called seaweed-like morphology, were firstly prepared via a simple method. The relatively large inter-fiber distances in the loose agglomerate allow unconstrained growth of metal oxide nanorods from the nanofibers throughout the whole

system, forming “hairy seaweed”, and at the same time the flexible, loose nanofiber agglomerate could easily take the shape of a container in aqueous media, offering the possibility to greatly increase the path length of the light and hence enhance the exposure of the active materials to the light. Zinc oxide (ZnO) is chosen as the active material in this work owing to its high carrier mobility, great chemical and thermal stability, and low toxicity. ZnO nanorods were conveniently grown on the surface of the PAN/ITO “seaweed” by hydrothermal route and the performance of such “hairy seaweed” was demonstrated as a photoanode in a PEC system.

Experimental section

Materials: Polyacrylonitrile (PAN, M_w = 150000), indium tin oxide nanopowder (ITO NP, < 50 nm), zinc acetate dehydrate ($Zn(CH_3COO)_2 \cdot 2H_2O$), zinc nitrate hexadydrate ($Zn(NO_3)_2 \cdot 6H_2O$), sodium sulfate (Na_2SO_4), and platinum (Pt) plate were obtained from Aldrich Chemistry (USA). Dimethylformamide (DMF) was purchased from Tedia Company Inc (USA). Ethanol was purchased from Fisher Chemical (UK). Ammonia solution (25 %) was purchased from Merck (Germany).

Electrospinning: PAN/ITO hybrid nanofibers (PITO NFs) were prepared via electrospinning using water as the collector. ITO NPs were dispersed into DMF (9 wt%) under vigorous ultrasonication. PAN was then dissolved in ITO/DMF suspension at the concentration of 6 wt% under continuing magnetic stirring at 60 °C. The above suspension was then electrospun into nanofibers at working voltage and feeding rate of 12 kV and 0.5 mL/h, respectively. Deionized water (DI H_2O) was used to collect the as-spun nanofibers with a distance of 15 cm between the needle tip and DI H_2O surface. After electrospinning for 20 and 40 min, respectively, a few drops of DI H_2O were used to wet the floated electrospun nanofibers. The nanofibers were then

suspended in the DI H_2O, forming a loosely agglomerated lump (Suspended-PITO). For comparison purpose, the lump was taken out from the DI H_2O, placed onto a glass slide and dried at 60 °C in vacuum. The dried mat is denoted as Dried-PITO.

Growth of ZnO nanorods: Suspended PITO was then transferred into 70 mL $Zn(NO_3)_2 \cdot 6H_2O$ aqueous solution (0.025 M) with 1.45 g ammonia solution (25 wt%) added. The growth was carried out in a Teflon-lined stainless steel autoclave at 90 °C for 24 hrs. After the hydrothermal treatment, the sample obtained was washed by DI H_2O several times and kept in DI H_2O for further use (Suspended-Z-PITO). For comparison purpose, Suspended-Z-PITO was taken out from the DI H_2O, placed onto a glass slide and dried at 60 °C in vacuum. The compact mat formed is denoted as Dried-Z-PITO.

Characterization: The morphologies of the samples were examined using a field emission scanning electron microscope (FESEM, JEOL 7600F) and a transmission electron microscope (TEM, JEOL 2100F). Elemental mapping was carried out using scanning TEM-energy dispersive X-ray spectroscope (STEM-EDX). Wide-angle X-ray diffraction (WAXD) measurements were carried out using a Bruker D8 Discover GADDS X-ray diffractometer with Cu Kα radiation. The light transmission (T, %), reflection (R, %) and absorption (A, %) of the samples which were loaded into blank cells were measured using a spectrophotometer (Lambda 950 UV/vis/NIR, PerkinElmer) in the wavelength range of 800 to 250 nm. Those of the corresponding blank cells filled with pure DI H_2O were also measured as references.

Photoelectrochemical measurement: Photoelectrochemical properties of the samples were measured using a three-electrode system. The prepared samples were used as working electrodes. A Pt sheet and Ag/AgCl standard electrode were used as counter and reference electrode,

respectively, with 0.5 M Na_2SO_4 aqueous solution as the electrolyte. The photocurrent-voltage tests were carried out using an electrochemical workstation (Autolab, PGSTAT302) within the voltage window of -0.2 to 0.3 V, and at the scanning rate of 0.1 V s^{-1}. The working electrodes were mounted on a copper (Cu) electrode and exposed to UV spot light source (LightingcureTM, model LC-5, from Hamamatsu Photonics, France, cf. Figure S1 for the light spectrum). The power density of the yielded illumination was 100 mW cm^{-2}.

Results and discussion

Preparation of 3D hierarchical nanostructures with hairy-seaweed-like morphology

The preparation process for such 3D hierarchical nanostructures with hairy-seaweed-like morphology is illustrated in Scheme 1. PAN/ITO hybrid nanofibers (PITO NFs) were prepared via conventional electrospinning of PAN/ITO/DMF suspension (cf. experimental section). In order to achieve 3D loose morphology, stationary DI H_2O was used to collect the PITO NFs, as shown in Scheme 1a. The as-spun PITO NFs could float on the surface of DI H_2O initially. After being wetted by a few drops of DI H_2O, the PITO NFs become suspended in the water, as displayed in Scheme 1b, forming a 3D loose lump (Suspended-PITO). FESEM studies show that PITO NFs have typical nanofiber morphology with few beads, while the surface of the nanofibers is fairly rough due to the embedded ITO nanoparticles (Figure 1a and 1b). The homogeneous distribution of ITO nanoparticles with size of tens of nanometers in the nanofibers is confirmed by the TEM image of a single PITO nanofiber (Figure 1c) and corresponding STEM-EDX elemental mappings (Figure $1d_1$~$1d_3$). It can be seen that due to the high content of ITO (feeding weight ratio of PAN/ITO = 40/60), these electrically conductive ITO nanoparticles are interconnected to one another, forming a continuous conduction pathway in the nanofibers.

Suspended-PITO NFs were then used as the skeletons to hydrothermally grow ZnO nanorods as ZnO nanorods are a promising candidate for photoanodes. The ITO nanoparticles on the surface of the nanofibers can act as nuclei for the growth of ZnO nanorods. Without the ITO nanoparticles, ZnO nanorods could hardly been grown on suspended pure PAN nanofibers following the same procedure (Figure S2), indicating the crucial role played by the ITO nanoparticles as seeds for the growth. Furthermore, the large inter-fiber distances in Suspended-PITO NFs allow unconstrained growth of ZnO nanorods throughout the whole system, whereas the growth of ZnO nanorods on compact nanofibrous mats occurs only on the surface of the mats (Figure S3). Scheme 1c shows the photo of a lump of the nanorods-on-nanofibers suspended in water (Suspended-Z-PITO), demonstrating that they are still in 3D loose form. Typical morphology of Suspended-Z-PITO is shown in Figure 2a and 2b. The ZnO nanorods are about 100 nm in diameter and 1 μm in length. They have hexagonal crystal structure, as evidenced by the WAXD results (Figure S4), and are densely, yet uniformly located on the surface of PITO NFs. TEM image (Figure 2c) and STEM-EDX elemental mapping (Figure $2d_1$~$2d_4$) of Z-PITO further confirm their dense branching morphology and element distribution. The high-resolution TEM image (Figure 2e) and diffraction pattern (Figure 2f) of a single ZnO nanorod indicate that each nanorod is a single crystal with inter-layer space of about 0.26 nm for (0002) planes.

Due to their seaweed-like loose morphologies in liquid media, both Suspended-PITO NFs and Suspended-Z-PITO can easily take the shape of a container, achieving macroscopic dimensions in all directions. Their interactions with light can therefore be greatly enhanced as the penetration depth of light in such suspended samples can be easily controlled by adjusting the dimension of the container in the direction parallel to the incident light (thickness direction). In order to verify this, quartz cells with different thicknesses, 5 mm and 10 mm, were used as path controller for

UV-visible light absorption measurements, as demonstrated in Figure 3a. To ensure a fair comparison, not only the thickness of the cell was controlled, the sample quantity was also controlled by fixing electrospinning duration, i.e., the nanofibers obtained from 20-min electrospinning were loaded into 5 mm-cell (Suspended-PITO-5mm and Suspended-Z-PITO-5mm), and the ones from 40-min electrospinning was loaded into 10 mm-cell (Suspended-PITO-10mm and Suspended-Z-PITO-10mm). In this way, the amount of material is also approximately doubled when the container thickness is doubled, ensuring that the two samples have similar loose morphology.

Optical properties of the seaweed-like nanostructures

The light transmission (T, %), reflection (R, %) and absorption (A, %) of Suspended-PITO with different thicknesses are shown in Figure 3b-3d, where the absorption was calculated by subtracting transmission and reflection from total incident light (100 %). For comparison purpose, those of Dried-PITO are also shown in the same figures. The measured reflection is mainly contributed by single reflections of the incident light from the nanofibers located on surface, as illustrated in Figure 3e. Therefore, when the thickness of Suspended-PITO is increased, the measured reflectance remains unchanged (Figure 3b). However, the suspended samples exhibit much lower reflectance than the dried one since the higher compactness of the dried sample makes more nanofibers be located on the surface and thus induces much severer single reflections. Taking out the loss caused by single reflections, the survived light can penetrate into the loosely suspended nanofiber samples and be effectively absorbed by the PITO NFs, which is assisted by multiple reflections from each individual suspended nanofiber inside the samples, as illustrated in Figure 3e. For Suspended-PITO, the probability of multiple reflections increases with thickness, strengthening the absorption and weakening the

transmission, as shown in Figure 3c and 3d. It is worth noting that the transmission of Suspended-Z-PITO-10mm is less than 5%, indicating that excluding the small loss caused by single reflections from the surface, almost all light can be absorbed by the nanofibers. By contrast, Dried-PITO shows the lowest absorption due to the large loss caused by its stronger single reflections from surface. The results shown in Figure S5 indicate that the DI H_2O-filled quartz cells exhibit high transmission of more than 90 %, low reflection of less than 10 % and almost no absorption within the wavelength range of 800 - 250 nm. This confirms that the cell filled with DI H_2O would not affect the optical measurement results significantly. It can thus be concluded that the nanofibers with such 3D loosely suspended morphology offers great advantages for effective and yet controllable UV-visible light absorption.

The optical properties of Suspended-Z-PITO were investigated using the same quartz cells and compared with that of Dried-Z-PITO. The results are shown in Figure 4. Since the surface of PITO NFs is almost fully covered by ZnO nanorods, the incident light, especially the UV light whose penetration depth (40 nm) is within the dimension of ZnO nanorods,[35] would be absorbed by and react with the ZnO nanorods rather than PITO NFs. It can be seen that the optical behaviours of Suspended-Z-PITO are similar to those of Suspended-PITO, e.g., the measured reflection remaining unchanged with the increase in thickness; having much lower reflection than that of Dried-Z-PITO; transmission decreasing and absorption increasing with the increase in thickness. The higher reflection of Suspended-Z-PITO than Suspended-PITO with same thickness is probably due to the optical property difference between PAN/ITO hybrid and ZnO. In addition to the multiple reflections induced by the loose, entangled nanofibrous morphology of Suspended-Z-PITO NFs, the multiple reflections between the randomly aligned ZnO nanorods may also help to further trap the light, resulting in an increase in interaction sites

of ZnO with light (Figure 4d). More electrochemically active materials, ZnO, are therefore exposed to light when increasing the sample thickness, promoting the photoelectrochemical reactions.

Photoelectrochemical properties of the hairy-seaweed-like nanostructures

To evaluate its PEC performance, Suspended-Z-PITO was used as a photoanode. A Cu sheet was used as the current collector, as shown schematically in Figure 5a. To clarify the effect of Cu, a bare Cu sheet was firstly used as the working electrode to measure photocurrent. Without light illumination, no photocurrent is generated from the Cu sheet until the applied potential reaches about 0.15 V (Figure 5b). Above this potential, a photocurrent is generated by the oxidation of the bare Cu sheet as the standard oxidation potential of Cu in neutral solution is +0.340 V, i.e., ~ 0.15 V vs. Ag/AgCl reference electrode.[36] After projecting light on the Cu sheet, the oxidation potential reduces and the short-circuit photocurrent density (J_{SC}) exhibited is 0.23 mA cm^{-2}.

The photocurrent density-voltage (*J-V*) curves of Suspended-Z-PITO with different thicknesses show characteristic semiconductor behavior under illumination (Figure 5b). It is shown clearly that Suspended-Z-PITO NFs give significantly higher photocurrent density than the bare Cu sheet, and the photocurrent density increases with sample thickness. For instance, the J_{SC} is 0.70 mA cm^{-2} for Suspended-Z-PITO-5mm, while it is as high as 1.0 mA cm^{-2} for Suspended-Z-PITO-10mm (inset of Figure 5b). The significantly higher J_{SC} of Suspended-Z-PITO than that of the bare Cu sheet is due to the photocurrent generated by the ZnO nanorods that are photoelectrochemically active. The high photocurrent density generated from Suspended-Z-PITO NFs can be attributed to their excellent light absorption and charge transport capabilities brought by their 3D loose morphology and 1D continuous conduction pathways, respectively. On one

hand, the 3D porous morphology of Z-PITO NFs provides high specific surface area, benefiting light absorption and interaction with the electrolyte. On the other hand, the incorporated ITO nanoparticles at a high content of 60 wt% in PITO NFs construct conductive pathways for the collection of charge carriers, significantly increasing the charge mobility and inhibiting the recombination of electrons and holes, as shown schematically in Figure 5a. The increase of photocurrent density with the increase in sample thickness is mainly due to the strengthened light trapping capability as mentioned above. The produced high photocurrent density indicates the great potential of such hairy-seaweed-like hierarchical nanostructures for PEC systems. As a subject of future studies, the investigation of their photoelectrochemical water splitting or photocatalytic properties can be carried out by simply growing other proper 1D active materials instead of ZnO.

Conclusions

In summary, highly porous 3D hierarchical nanostructures suspended in aqueous media, Suspended-Z-PITO NFs, have been facilely prepared via electrospinning of PAN/ITO nanofibers and collection of the nanofibers by water, followed by hydrothermally growing ZnO nanorods from the nanofibers. The large inter-fiber distances facilitate the uniform growth of the ZnO nanorods throughout the whole system. These 3D centimeter-sized novel hierarchical nanostructures possess excellent light absorption capability owing to their large thickness and intensive multiple reflections inside. High photocurrent densities are achieved when Suspended-Z-PITO NFs are used as photoanodes. The high photocurrent densities achieved can be attributed to the largely increased number of light-ZnO interaction sites brought by the excellent light-trapping capability, large contact area of the ZnO nanorods with the electrolyte, as well as the conduction paths formed by the ITO nanoparticles.

ASSOCIATED CONTENT

Supporting Information. Spectrum of the spot light source, SEM images of growth of ZnO nanorods on pure PAN nanofibers and compact PAN/ITO nanofibrous mat, WAXD patterns of PAN/ITO nanofibers and ZnO-PAN/ITO nanofibers and optical properties of blank cells filled with DI H_2O. This material is available free of charge via the Internet at http://pubs.acs.org.

AUTHOR INFORMATION

Corresponding Author

*E-mail: asxhlu@ntu.edu.sg

Author Contributions

[§]These authors contributed equally.

REFERENCES

1. H. M. Chen, C. K. Chen, R. S. Liu, L. Zhang, J. Zhang, D. P. Wilkinson, *Chem. Soc. Rev.* **2012**, *41*, 5654-5671.

2. J. Brillet, M. Gratzel, K. Sivula, *Nano Lett.* **2010**, *10*, 4155-4160.

3. P. Hartmann, D.-K. Lee, B. M. Smarsly, J. Janek, *ACS Nano* **2010,** *4*, 3147-3154.

4. H. Ishihara, G. K. Kannarpady, K. R. Khedir, J. Woo, S. Trigwell, A. S. Biris, *Phys. Chem. Chem. Phys.* **2011**, *13*, 19553-19560.

5. C. X. Kronawitter, S. S. Mao, B. R. Antoun, *Appl. Phys. Lett.* **2011**, *98*, 092108-3.

6. L. Ren, L. Jin, J. B. Wang, F. Yang, M. Q. Qiu, Y. Yu, *Nanotechnol.* **2009**, *20*, 115603(9pp).

7. D. D. Elia, C. Beauger, J. F. Hochepied, A. Rigacci, M. H. Berger, N. Keller, V. Keller-Spitzer, Y. Suzuki, J. C. Valmalette, M. Benabdesselam, P. Achard, *Int. J. Hydrog. Energy* **2011**, *36*, 14360-14373.

8. R. Q. Zhang, X. M. Liu, Z. Wen, Q. Jiang, *J. Phys. Chem. C* **2011**, *115*, 3425-3428.

9. N. K. Allam, A. J. Poncheri, M. A. El-Sayed, *ACS Nano* **2011**, *5*, 5056-5066.

10. Q. P. Ding, Y. P. Yuan, X. Xiong, R. P. Li, H. B. Huang, Z. S. Li, T. Yu, Z. G. Zou, S. G. Yang, *J. Phys. Chem. C* **2008**, *112*, 18846-18848.

11. J. Ng, S. P. Xu, X. W. Zhang, H. Y. Yang, D. D. Sun, *Adv. Funct. Mater.* **2010**, *20*, 4287-4294.

12. T. Krishnamoorthy, V. Thavasi, M. Subodh G, S. Ramakrishna, *Energy Environ. Sci.* **2011**, *4*, 2807.

13. S. Cavaliere, S. Subianto, I. Savych, D. J. Jones, J. Roziere, *Energy Environ. Sci.* **2011**, *4*, 4761.

14. C. Zhen, G. Liu, H. M. Cheng, *Nanoscale* **2012**, *4*, 3871-3874.

15. C. Y. Cummings, F. Marken, L. M. Peter, K. G. U. Wijayantha, A. A. Tahir, *J. Am. Chem. Soc.* **2012**, *134*, 1228-1234.

16. A. Wolcott, W. A. Smith, T. R. Kuykendall, Y. Zhao, J. Z. Zhang, *Adv. Funct. Mater.* **2009**, *19*, 1849-1856.

17. A. Stepanovich, K. Sliozberg, W. Schuhmann, A. Ludwig, *Int. J. Hydrog. Energy* **2012**, *37*, 11618-11624.

18. Q. X. Jia, K. Iwashina, A. Kudo, *Proc. Natl. Acad. Sci. U. S. A.* **2012**, *109*, 11564-11569.

19. P. S. Shinde, G. H. Go, W. J. Lee, *J. Mater. Chem.* **2012,** *22*, 10469-10471.

20. K. S. Ahn, Y. Yan, S. Shet, J. Kim, T. Deutsch, J. Turner, A. J. Mowafak, *Appl. Phys. Lett.* **2008**, *93*, 163117-3.

21. B. D. Chernomordik, H. B. Russell, U. Cvelbar, J. B. Jasinski, V. Kumar, T. Deutsch, M. K. Sunkara, *Nanotechnol.* **2012,** *23*, 194009 (9pp).

22. H. M. Chen, C. K. Chen, C. C. Lin, R. S. Liu, H. Yang, W. S. Chang, K. H. Chen, T. S. Chan, J. F. Lee, D. P. Tsai, *J. Phys. Chem. C* **2011**, *115*, 21971-21980.

23. H. M. Chen, C. K. Chen, Y. C. Chang, C. W. Tsai, R. S. Liu, S. F. Hu, W. S. Chang, K. H. Chen, *Angew. Chem. Int. Ed.* **2010**, *49*, 5966-5969.

24. Y. F. Wei, L. Ke, J. H. Kong, H. Liu, Z. H. Jiao, X. H. Lu, H. J. Du, X. W. Sun, *Nanotechnol.* **2012**, *23*, 235401(8pp).

25. N. Chouhan, C. L. Yeh, S. F. Hu, R. S. Liu, W. S. Chang, K. H. Chen, *Chem. Commun.* **2011**, *47*, 3493-3945.

26. S. Z. Liang, J. F. He, Z. H. Sun, Q. H. Liu, Y. Jiang, H. Cheng, B. He, Z. Xie, S. Q. Wei, *J. Phys. Chem. C* **2012**, *116*, 9049-9053.

27. J. Shi, Y. Hara, C. L. Sun, M. A. Anderson, X. D. Wang, *Nano Lett.* **2011**, *11*, 3413-3419.

28. H. Kim, M. Seol, J. Lee, K. Yong, *J. Phys. Chem. C* **2011**, *115*, 25429-25436.

29. Z. Zhang, P. Wang, *Energy Environ. Sci.* **2012**, *5*, 6506-6512.

30. J. Shi, X. Wang, *Energy Environ. Sci.* **2012**, *5*, 7918-7922.

31. I. S. Cho, Z. B. Chen, A. J. Forman, D. R. Kim, P. M. Rao, T. F. Jaramillo, X. L. Zheng, *Nano Lett.* **2011**, *11*, 4978-4984.

32. J. H. Qiu, M. Guo, Y. J. Feng, X. D. Wang, *Electrochim. Acta* **2011**, *56*, 5776-5782.

33. Y. Qiu, K. Yan, H. Deng, S. Yang, *Nano Lett.* **2011**, *12*, 407-413.

34. J. Kong, S. Y. Wong, Y. Zhang, H. R. Tan, X. Li, X. Lu, *J. Mater. Chem.* **2011**, *21*, 15928.

35. I. S. Jeong, J. H. Kim, S. Im, *Appl. Phys. Lett.* **2003**, *83*, 2946-2948.

36. A. J. Bard, R. Parsons, J. Jordan, Standard Potentials in Aqueous Solutions, Marcel Dekker: New York, **1985**, pp287-293.

Scheme 1. A scheme showing sample preparation process. (a) Electrospinning setup with water collector, (b) and (c) morphology of the obtained 3D porous lump suspended in DI H_2O.

Figure 1. (a, b) FESEM and (c) TEM images of PAN/ITO hybrid nanofibers (PITO NFs), and (d_1~d_3) the corresponding STEM-EDX elemental mapping of a single PITO nanofiber.

Figure 2. (a) and (b) FESEM images of PAN/ITO hybrid nanofibers with grown ZnO nanorods (Z-PITO NFs). (c) TEM image and (d_1~d_4) STEM-EDX elemental mapping of Z-PITO NFs. (e) High-resolution TEM image and (f) diffraction pattern of a single ZnO nanorod.

Figure 3. (a) Pictures of the quartz cells loaded with Suspended-PITO. UV-visible light (b) reflection, (c) transmission and (d) absorption of Suspended-PITO with different thicknesses and Dried-PITO mat. (e) Schematic illustration of single reflection from the surface and multiple reflections between individual suspended PITO nanofibers.

Figure 4. UV-visible light (a) reflection, (b) transmission and (c) absorption of Suspended-Z-PITO with different thicknesses and Dried-Z-PITO. (d) Schematic illustration of multiple reflections between ZnO nanorods on the nanofibers (cross-sectional view).

Figure 5. (a) Schematic illustration of photocurrent generation process from Suspended-Z-PITO NFs with a Cu sheet as the current collector. (b) Photocurrent density-voltage (*J-V*) characteristics of Suspended-Z-PITO NFs with thickness of 5 mm (Suspended-Z-PITO-5mm) and 10 mm (Suspended-Z-PITO-10mm), respectively, as well as that of the bare Cu sheet, in dark and under illumination. The inset shows the enlarged *J-V* curves in the voltage window of -0.05~0.023 V.

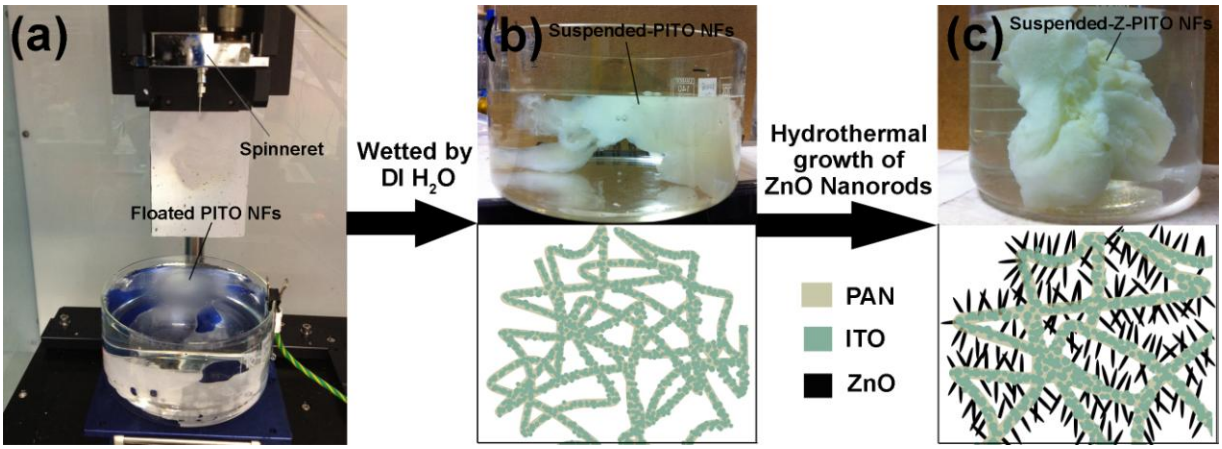

Scheme 1. A scheme showing sample preparation process. (a) Electrospinning setup with water collector, (b) and (c) morphology of the obtained 3D porous lump suspended in DI H_2O.

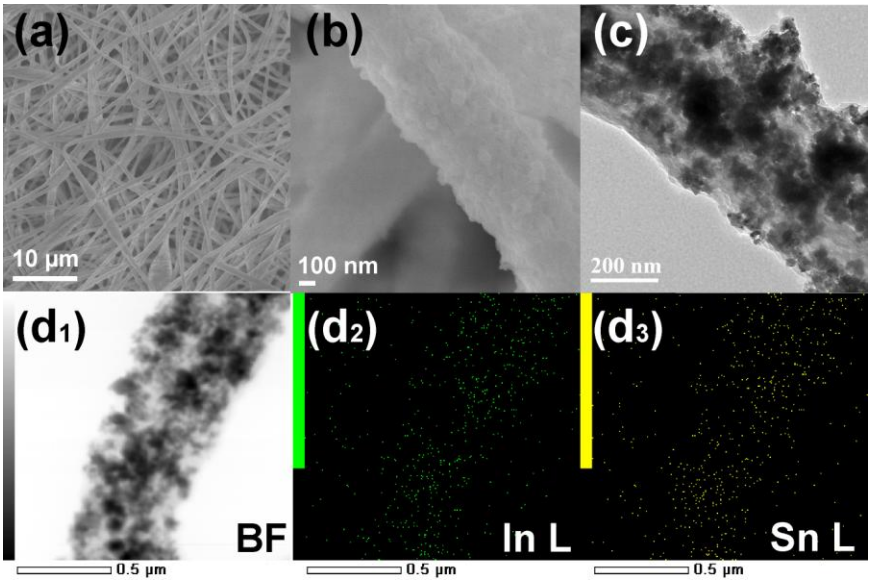

Figure 1. (a, b) FESEM and (c) TEM images of PAN/ITO hybrid nanofibers (PITO NFs), and (d_1~d_3) the corresponding STEM-EDX elemental mapping of a single PITO nanofiber.

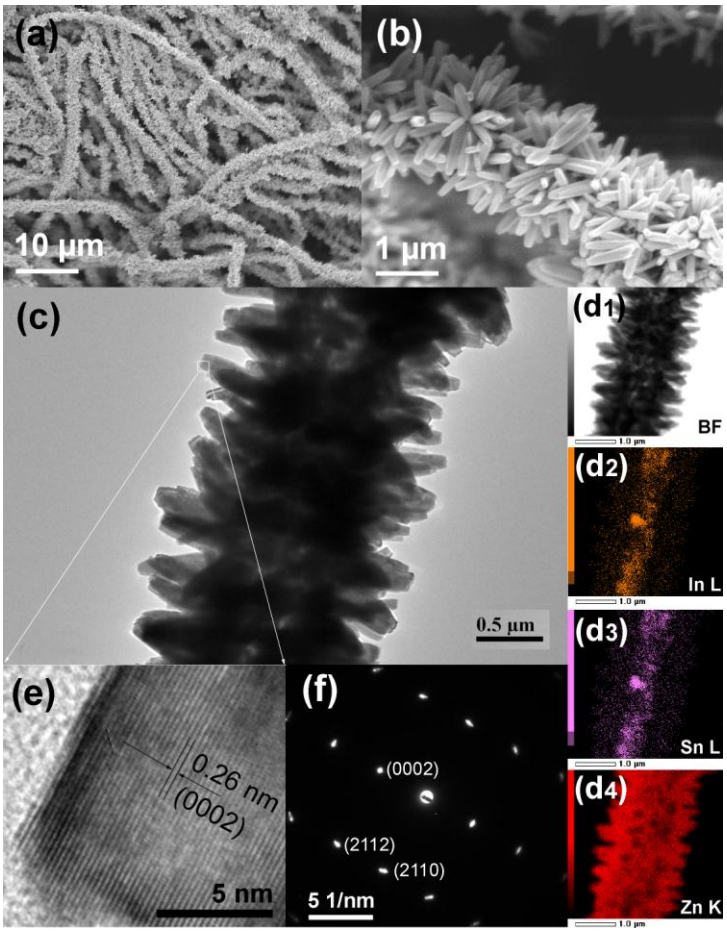

Figure 2. (a) and (b) FESEM images of PAN/ITO hybrid nanofibers with grown ZnO nanorods (Z-PITO NFs). (c) TEM image and (d_1~d_4) STEM-EDX elemental mapping of Z-PITO NFs. (e) High-resolution TEM image and (f) diffraction pattern of a single ZnO nanorod.

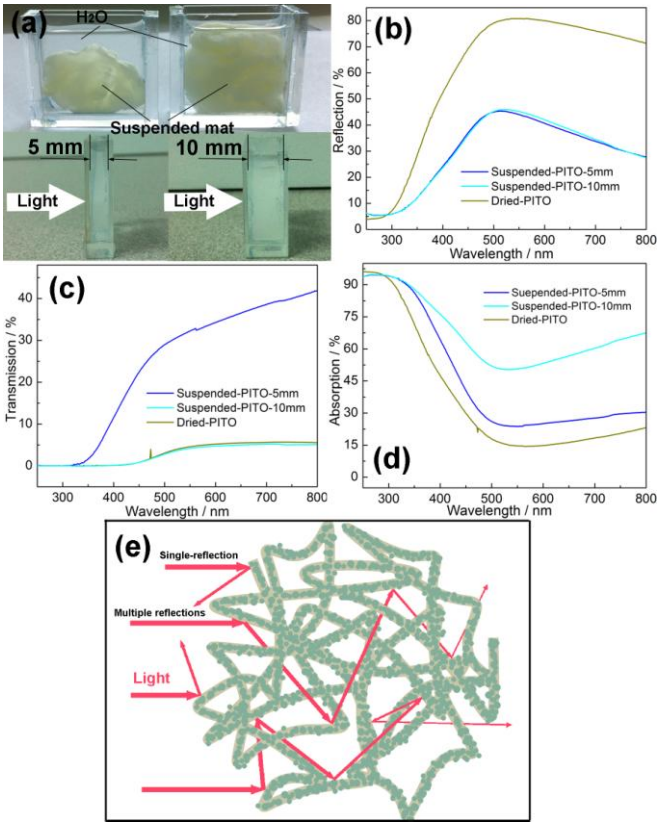

Figure 3. (a) Pictures of the quartz cells loaded with Suspended-PITO. UV-visible light (b) reflection, (c) transmission and (d) absorption of Suspended-PITO with different thicknesses and Dried-PITO mat. (e) Schematic illustration of single reflection from the surface and multiple reflections between individual suspended PITO nanofibers.

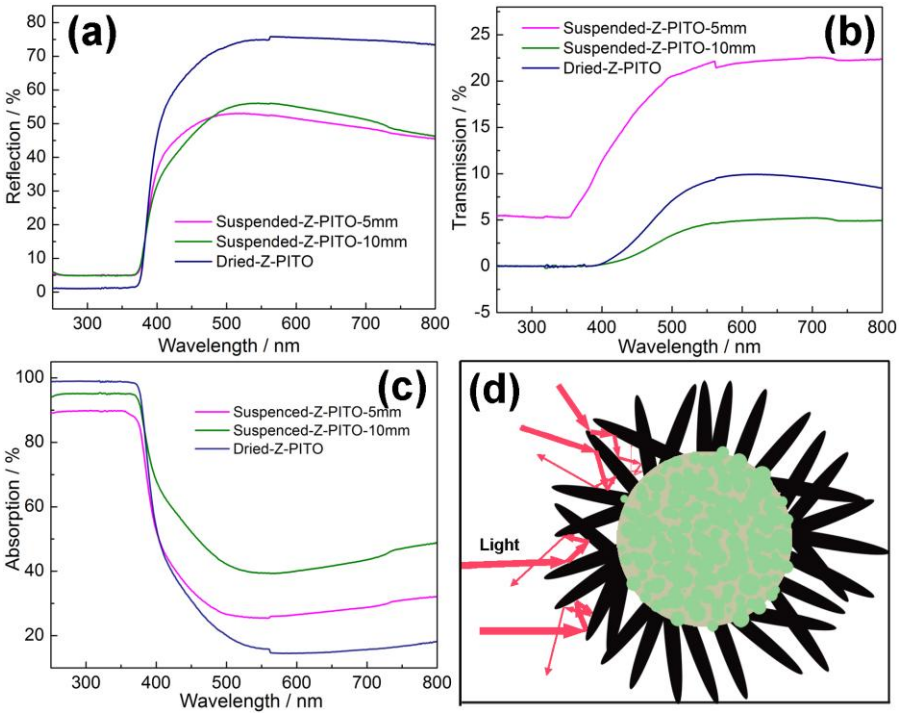

Figure 4. UV-visible light (a) reflection, (b) transmission and (c) absorption of Suspended-Z-PITO with different thicknesses and Dried-Z-PITO. (d) Schematic illustration of multiple reflections between ZnO nanorods on the nanofibers (cross-sectional view).

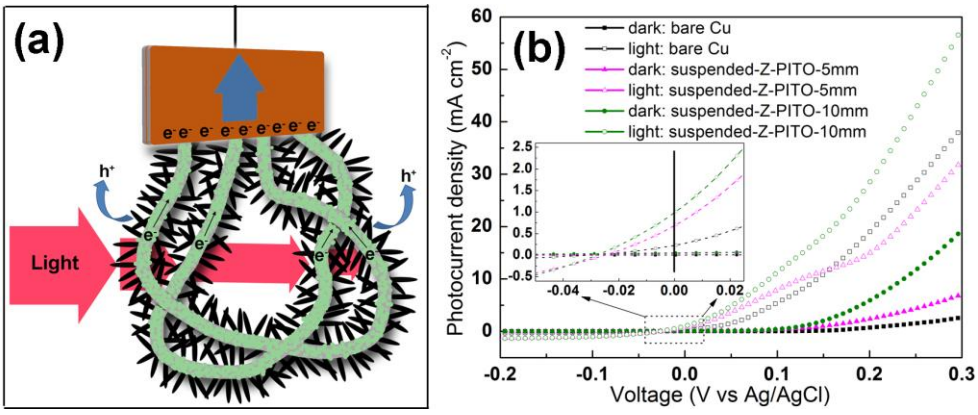

Figure 5. (a) Schematic illustration of photocurrent generation process from Suspended-Z-PITO NFs with a Cu sheet as the current collector. (b) Photocurrent density-voltage (*J-V*) characteristics of Suspended-Z-PITO NFs with thickness of 5 mm (Suspended-Z-PITO-5mm)

and 10 mm (Suspended-Z-PITO-10mm), respectively, as well as that of the bare Cu sheet, in dark and under illumination. The inset shows the enlarged *J-V* curves in the voltage window of -0.05~0.023 V.

Table of Contents graphic